

Prospects for measurement and control of the scattering length of metastable helium using photoassociation techniques

J.C.J. Koelemeij^a and M. Leduc^b

École Normale Supérieure and Collège de France, Laboratoire Kastler Brossel, 24 rue Lhomond, 75231 Paris Cedex 05, France

Received 3rd July 2004

Published online 23 November 2004 – © EDP Sciences, Società Italiana di Fisica, Springer-Verlag 2004

Abstract. A numerical investigation of two-laser photoassociation (PA) spectroscopy on spin-polarized metastable helium (He^*) atoms is presented within the context of experimental observation of the least-bound energy level in the scattering potential and subsequent determination of the s -wave scattering length. Starting out from the model developed by Bohn and Julienne [Phys. Rev. A **60**, 414 (1999)], PA rate coefficients are obtained as a function of the parameters of the two lasers. The rate coefficients are used to simulate one- and two-laser PA spectra. The results demonstrate the feasibility of a spectroscopic determination of the binding energy of the least-bound level. The simulated spectra may be used as a guideline when designing such an experiment, whereas the model may also be employed for fitting experimentally obtained PA spectra. In addition, the prospects for substantial modification of the He^* scattering length by means of optical Feshbach resonances are considered. Several experimental issues relating to the numerical investigation presented here are discussed.

PACS. 34.20.Cf Interatomic potentials and forces – 32.80.Pj Optical cooling of atoms; trapping – 34.50.Gb Electronic excitation and ionization of molecules; intermediate molecular states (including lifetimes, state mixing, etc.)

1 Introduction

Within the context of ultracold quantum gases, Bose-Einstein condensation (BEC) of metastable helium has opened up the way for experiments exploiting the 19.8 eV internal energy of the He^* atoms in novel detection schemes [1–3]. The accuracy of the results obtained in contemporary experiments, however, is compromised by the lack of an accurate determination of the value of the He^* s -wave scattering length [4–8]. Another limitation in ultracold He^* experiments is the absence of magnetic Feshbach resonances to control the interaction between the atoms, which is a consequence of the zero nuclear spin of ^4He .

Standard techniques based on photoassociation (PA) spectroscopy have enabled accurate determination of the scattering length for most alkali elements. For the experimental determination of the scattering length two widely-used methods exist. The first one relies on determining the binding energy of the least-bound level in the scattering potential via a stimulated two-photon Raman transition, from which the scattering length can be inferred (see, for

instance, Refs. [9,10]). This method is schematically depicted in Figure 1. In the second method, Franck-Condon oscillations observed in the line strength of transitions from the free-particle ground state to vibrational levels in an electronically excited molecular state are used to determine the nodes in the scattering wavefunction, from which the scattering length may also be deduced [11].

For the case of two spin-polarized 2^3S_1 helium atoms, elastic scattering takes place in a $^5\Sigma_g^+$ potential. However, the application of standard techniques to locate the least-bound state in this potential is not entirely straightforward. The situation is complicated by the autoionization of metastable helium dimers, which occurs at short internuclear range. Only dimers in a pure quintet spin configuration at short range will experience suppression of autoionization such that well-resolved vibrational resonances exist. This reduces a priori the number of useful pathways for a PA experiment. In addition, the short-lived singlet and triplet vibrational states effectively merge into a continuum which may result in unwanted background signal during PA experiments. Indeed, long-lived vibrational levels have recently been observed in molecular states which possess quintet character at short internuclear range [12,13]. Some of these states, which are located below the D_2 ($2^3\text{S}_1 + 2^3\text{P}_2$) asymptote, might be useful

^a Present address: Time and Frequency Division, National Institute of Standards and Technology, 325 Broadway, Boulder, Colorado 80305, USA.

^b e-mail: leduc@physique.ens.fr

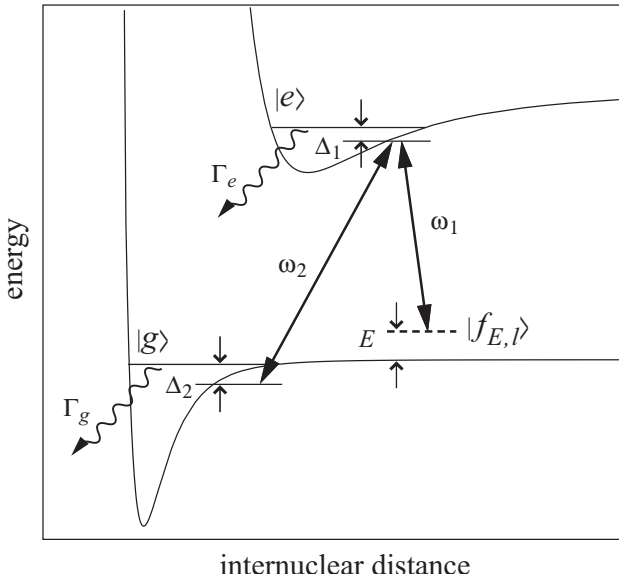


Fig. 1. Schematic view of two-laser photoassociation, employed here to convert a pair of free atoms (denoted as $|f_{E,l}\rangle$) into the least bound molecular state $|g\rangle$ supported by the scattering potential.

intermediate levels for a two-laser PA experiment aiming at the determination of the energy of the least-bound level in the scattering potential.

An interesting alternative is offered by vibrational levels in the purely long-range 0_u^+ potential well below D_0 ($2\ ^3S_1 + 2\ ^3P_0$), observed by Léonard et al. [13–15]; see also Figure 2. For such states the classical inner turning point lies at long range, which leads to total inhibition of the short-range autoionization process. Despite their long-range location, the vibrational wavefunctions can be estimated to have sufficient Franck-Condon (FC) overlap with the least-bound wavefunction in the $^5\Sigma_g^+$ potential. The $^5\Sigma_g^+$ potential has been calculated ab initio by Stärck and Meyer [16], from which a scattering length of $150\ a_0$ is inferred. Gadea et al. reconsidered the same potential and concluded that the least-bound vibrational level must be $v = 14$, with a binding energy of at least $-10\ \text{MHz}$ [4]. This translates to a scattering length smaller than $340\ a_0$. By comparison, the most accurate experimental value for the He^* scattering length to date (which was obtained by observing inelastic collisions at BEC threshold) is $195_{-20}^{+40}\ a_0$ [7], in agreement with the theoretical prediction.

Control of the value of the scattering length may be achieved by means of an *optical* Feshbach resonance (OFR), as first proposed by Fedichev et al. [17], and recently observed by Theis et al. [18]. It was pointed out that a laser coupling a colliding pair of ultracold atoms to a bound level in an excited molecular state may cause a significant modification of the scattering length. This scheme, however, also implies loss of trapped atoms after spontaneous decay of the excited state. A suitable combination of experimental parameters should be chosen to minimize these losses.

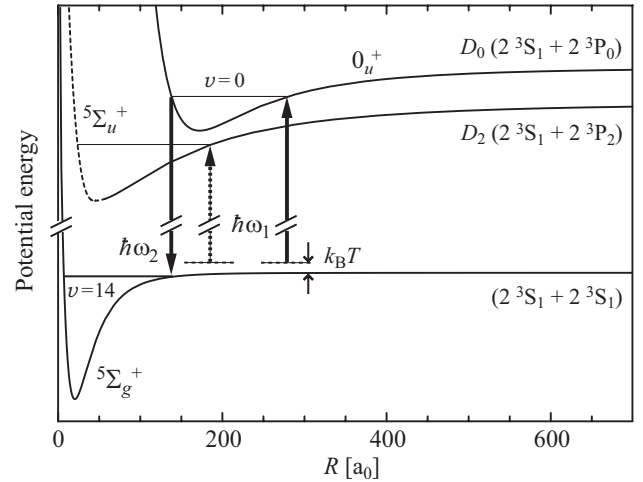


Fig. 2. PA of spin-polarized He^* atoms. Laser 1 (dashed arrow) can couple two free atoms (which are initially in the $^5\Sigma_g^+$ scattering potential) to an excited bound state, for instance in the potential correlating to the D_2 asymptote, thereby creating an OFR. The dashed short-range part of the potential well indicates that it is not accurately known. Laser 1 may also be tuned to $v = 0$ vibrational state in the purely long range 0_u^+ potential below the D_0 asymptote (solid arrow). Laser 2 may then resonantly couple this state to the least-bound ($v = 14$) vibrational state in the $^5\Sigma_g^+$ scattering potential. The difference frequency of the two lasers is directly related to the binding energy of the $v = 14$ state.

Both two-laser PA and optical Feshbach resonances can be investigated numerically using a scattering model derived within the framework of generalized multichannel quantum defect theory, as done by Bohn and Julienne [19]. Their results, which are recapitulated in Section 2, include scattering matrix elements and a recipe for calculating two-laser PA rate coefficients. In Section 3.1, two-laser PA spectra are simulated for the circumstances pertaining to the experiment described in references [14,15]. Next, in Section 3.2, an account of the achievable modification of the He^* scattering length using an OFR is given. In addition, experimental issues which may play a role in the choice of a suitable vibrational level for the OFR are discussed. Conclusions are presented in Section 4.

2 Theoretical background

2.1 Two-laser photoassociation

Experimentally, PA spectra are obtained by monitoring the production rate of a certain product P resulting from the decay of the level being populated, while scanning the frequency of the PA laser. For instance, P could be the photon emitted during spontaneous decay. Plotting the rate coefficient associated with the production of P , K_P , versus the PA laser frequency therefore simulates the PA spectrum. For a two-laser PA experiment involving a collection of atoms characterized by a Maxwell-Boltzmann

energy distribution, K_P can be expressed as [20]

$$K_P(T, \omega_1, \omega_2, I_1, I_2) = (2\pi\hbar Q_T)^{-1} \sum_{l=0}^{\infty} (2l+1) \times \int_0^{\infty} |S_P(E, l, \omega_1, \omega_2, I_1, I_2)|^2 e^{-E/k_B T} dE. \quad (1)$$

Here, the integration is over all initial scattering energies E . $|S_P(E, l, \omega_1, \omega_2, I_1, I_2)|^2$ is the squared absolute value of the S -matrix element, which represents the probability of production of P as a function of the frequencies ω_1, ω_2 and intensities I_1, I_2 of lasers 1 and 2, respectively. The summation index l labels the partial wave contributing to the scattering process, and $Q_T = (\mu k_B T / 2\pi\hbar^2)^{3/2}$ is the translational partition function with μ denoting the reduced mass of the system. For the two-laser case, there are three possibilities for the final state after the scattering process. These correspond to the transition of the initial free-atom pair (denoted as an energy-normalized state $|f_{E,l}\rangle$) to the excited state $|e\rangle$, the bound molecular ground state $|g\rangle$, or back to $|f\rangle$ (see also Fig. 1). For the case of PA of He^* , the term ‘‘ground state’’ refers to the metastable ($2\ ^3\text{S} + 2\ ^3\text{S}$) $^5\Sigma_g^+$ state, and not to the actual ground state of the helium dimer. The probability for each of these transitions to take place is determined by the squared absolute value of the corresponding S -matrix element, the explicit form of which is given in equations (4.8–4.11) of reference [19]. The S -matrix elements themselves depend on the rate γ_s of stimulated free-to-bound transitions induced by laser 1, the bound-bound Rabi coupling by laser 2, Ω , the decay widths Γ_e and Γ_g of the excited and ground molecular bound states, respectively, and the detunings Δ_1 and Δ_2 of lasers 1 and 2. The detunings are defined as $\Delta_1 = E_e/\hbar - \omega_1$ and $\Delta_2 = E_g/\hbar - (\omega_1 - \omega_2)$, where E_e and E_g are the energies (with respect to the $2\ ^3\text{S} + 2\ ^3\text{S}$ asymptote) of the excited-state and ground-state vibrational levels, respectively. This definition of the detuning implies that a negative value for Δ_i corresponds to a *blue* detuning. The stimulated rate γ_s is obtained from Fermi’s golden rule:

$$\gamma_s = (2\pi/\hbar) |\langle f_{E,l} | V_{\text{rad}} | e \rangle|^2, \quad (2)$$

where the radiative coupling, V_{rad} , by laser 1 is given by

$$V_{\text{rad}} = d \left(\frac{I_1}{\epsilon_0 c} \right)^{1/2}. \quad (3)$$

Here, d is the *atomic* dipole moment operator, and the polarization of the light is ignored for the moment. It should be mentioned that the use of energy-normalized states automatically includes the correct Wigner law threshold behaviour, which means that γ_s vanishes as $E^{(2l+1)/2}$ for $E \rightarrow 0$.

V_{rad} also determines the Rabi coupling between the ground and excited bound states, and the Rabi frequency, Ω , is given by

$$\Omega = \langle e | V_{\text{rad}} | g \rangle / \hbar. \quad (4)$$

2.2 Optical Feshbach resonance

To create an optical Feshbach resonance, only one PA laser is required. The S -matrix elements for two-laser PA may also be used to describe PA by a single laser by setting the intensity of laser 2 to zero. Then, from the scattering matrix element S_{00} for elastic scattering (see Eqs. (4.9–4.11) in Ref. [19]) a complex-valued phase shift, δ , may be obtained using the relation [21]

$$S_{00} = \exp(2i\delta). \quad (5)$$

For low scattering energies, this complex phase shift translates to a complex-valued scattering length, a , according to

$$a = A - iB \equiv - \lim_{k \rightarrow 0} \frac{1}{k} \tan \delta. \quad (6)$$

Here, $k = \sqrt{2\mu E/\hbar^2}$ denotes the initial wave number. Using the explicit expression for S_{00} given in reference [19], it can be shown that

$$A = a_{\text{nat}} + \frac{1}{2k} \frac{\gamma_s [E - \hbar\Delta_1 - E(I_1)]}{[E - \hbar\Delta_1 - E(I_1)]^2 + (\Gamma_e/2)^2}, \quad (7)$$

where a_{nat} is the natural value of the scattering length, and

$$B = \frac{1}{4k} \frac{\gamma_s \Gamma_e}{[E - \hbar\Delta_1 - E(I_1)]^2 + (\Gamma_e/2)^2}. \quad (8)$$

Here, $E(I_1)$ is an energy- and intensity-dependent frequency shift [19], which will be ignored below as it does not fundamentally change the results. The imaginary part of a accounts for losses due to spontaneous emission occurring in the excited state. By tuning the intensity and/or the detuning from the resonance, a may be varied. It should be noted that within this picture, mixing due to state dressing of the initial free state and the excited bound state is ignored. This has been predicted to give rise to additional frequency shifts and even extra resonances for PA at relatively high intensity [22, 23].

The real and imaginary parts of a can be converted into rate coefficients, K_{el} and K_{inel} , for elastic and inelastic collisions, respectively [21]:

$$K_{\text{el}} = \frac{8\pi\hbar}{\mu} k (A^2 + B^2), \quad K_{\text{inel}} = \frac{8\pi\hbar}{\mu} B. \quad (9)$$

Here, K_{inel} relates to scattering events in which two atoms are lost (in Sect. 3.2 the various loss processes will be described).

3 Numerical results

3.1 Two-laser photoassociation spectra

As has been pointed out in reference [14], the $v = 0, J = 1$ state in the 0_u^+ potential well below D_0 (Fig. 2) is expected to have sufficient FC overlap with the least-bound

state in the ${}^5\Sigma_g^+$ scattering potential. The value of the squared FC-overlap integral is of the order of 10^{-1} (which is more than one order of magnitude larger than for any of the other five bound states observed in the 0_u^+ well), for which case the efficiency of the second step in the two-laser PA process should be reasonable. The fact that the $v = 0, J = 1$ line could be observed with a good signal-to-noise (S/N) ratio indicates that also the first step can be made at a sufficiently high rate [14]. For the simulation of two-laser PA, the $v = 0, J = 1$ state will be used as the intermediate state, and conditions similar to those in the experiments described in references [14,15] will be assumed. These imply PA on a magnetostatically trapped cloud consisting of 10^5 – 10^6 spin-polarized He* atoms, at densities 10^{12} – 10^{13} cm^{-3} , and temperatures 10–100 μK . It was checked that for such low temperatures, all $l \geq 2$ contributions to the summation in equation (1) are negligibly small as compared to the s -wave contribution. Since odd partial waves do not contribute to the scattering of identical bosonic He* atoms, only the $l = 0$ term is retained. This is consistent with the fact that no vibrational levels in 0_u^+ with total rotational quantum number $J > 1$ were observed experimentally [14,15].

For the evaluation of the matrix elements in equations (2) and (4), the wavefunctions of the involved states must be known. For the ${}^5\Sigma_g^+$ wavefunctions, these are obtained by numerically solving the radial Schrödinger equation using the potential data from reference [16]. Of course, the wavefunctions depend on the actual shape of the potential, which is not accurately known. For the simulation of two-laser PA spectra the above mentioned potential data are used. In case that the actual potential turns out to deviate from the one used here, the difference between the two potentials will predominantly affect the radiative coupling (Eq. (3)) via the FC overlap of the radial wavefunctions (see also the Appendix). However, for most potential curves lying within the range of the theoretical prediction, the differences due to this effect will not be too large. Also the 0_u^+ wavefunction is found by numerical integration of the Schrödinger equation, using the Born-Oppenheimer potential obtained from diagonalization of the long-range interaction between a 2^3S and a 2^3P atom. Here, the long-range interaction includes the electrostatic resonant dipole-dipole interaction (which scales with the internuclear distance R as R^{-3}), the van der Waals interaction (scaling as R^{-6}), and the atomic relativistic interactions (spin-orbit, spin-spin, etc.) [15]. Further details of the evaluation of the matrix elements are postponed to the appendix.

Having acquired all necessary information, equation (1) can be employed to calculate the rate coefficient K_f for observation of fluorescence decay of the excited state. In Figure 3a, K_f is plotted versus laser-frequency detuning for a single-laser PA experiment, and for various temperatures. For the 25 μK case, the line profile has a width close to the spontaneous decay width of ~ 3 MHz, which is about twice the width of the atomic $2^3\text{S}_1 \rightarrow 2^3\text{P}_0$ line [15]. For higher temperatures the line becomes increasingly more shifted, broadened and skewed.

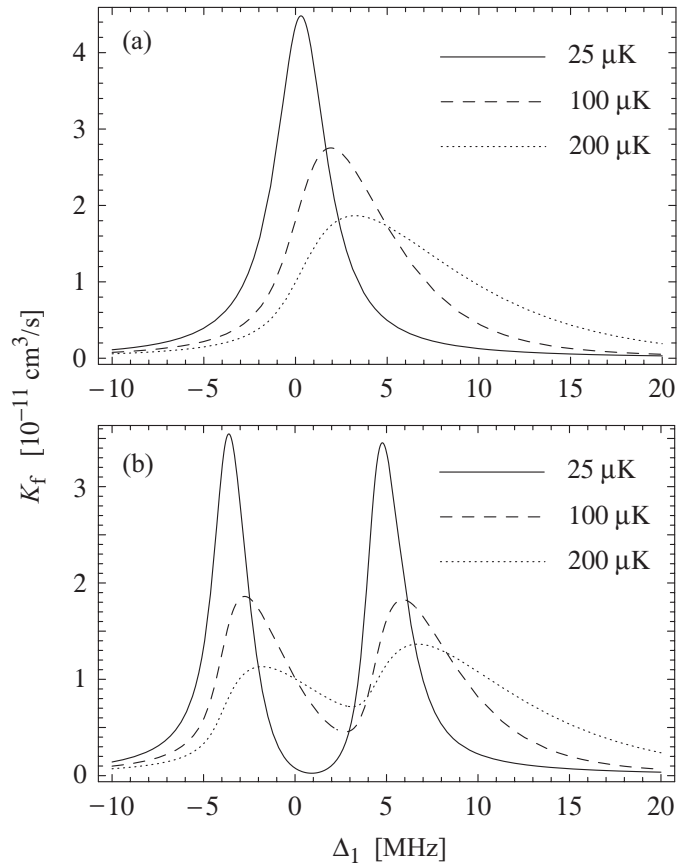


Fig. 3. Rate coefficients for observation of spontaneous emission from the excited state plotted as a function of Δ_1 , for various temperatures. (a) Single-laser line shapes with $I_1 = 100 I_{\text{sat}}$. (b) Two-laser line shapes, with $\Delta_2 = 0$, $I_1 = 100 I_{\text{sat}}$ and $I_2 = 400 I_{\text{sat}}$. The spectra in (b) correspond to the case of frustrated PA.

It also follows that for intensities well below $10^4 I_{\text{sat}}$ (with $I_{\text{sat}} = 1.67$ W/m^2 the saturation intensity of the atomic $2^3\text{S}_1 \rightarrow 2^3\text{P}_0$ transition), broadening due to saturation does not play a significant role. The bandwidth of the PA laser is neglected, which is justified for a laser with a few-hundred kHz bandwidth.

For the two-laser case depicted in Figure 3b, laser 1 is scanned across the Autler-Townes doublet induced by laser 2. Again, at higher temperatures the spectrum becomes more shifted, and the Autler-Townes doublet becomes less resolved. In Figure 4a, an example of stimulated two-photon Raman PA is depicted. Laser 2 is now detuned several linewidths below resonance, and scanning laser 1 from blue to red shows the “unperturbed” line and the narrow Raman line, respectively. The width of the latter is determined by the autoionization width of the ${}^5\Sigma_g^+$ state (see below), and by thermal broadening. An alternative approach for detecting the two-photon transition is shown in Figure 4b. Here, laser 1 is kept at the maximum of the single-laser line (i.e. $\Delta_1 \approx 0$), whereas laser 2 is scanned. As long as laser 2 is not resonant, a background signal due to PA will be present. When laser 2 becomes resonant, the single-laser line will split up into the

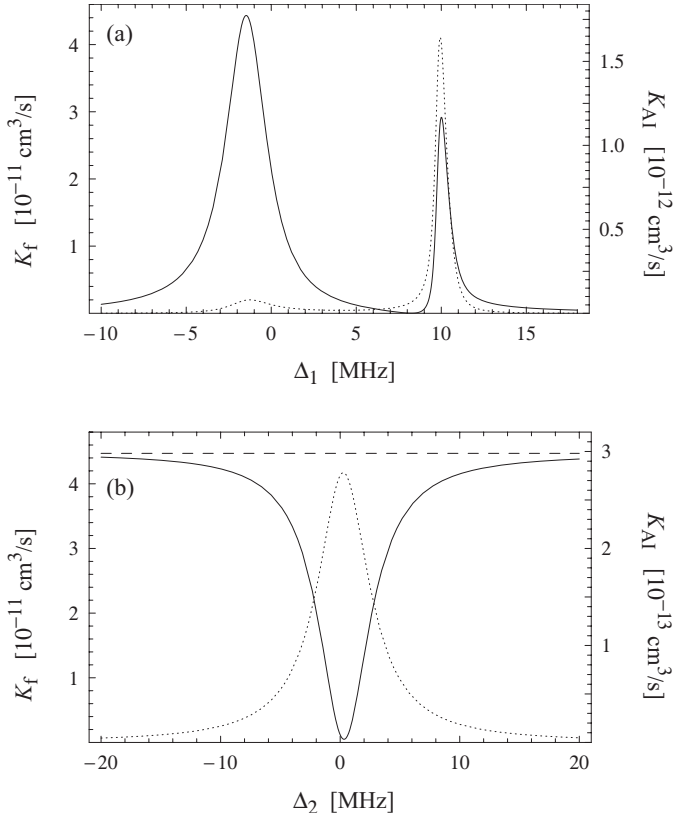


Fig. 4. Rate coefficients for observation of fluorescence decay (K_f , solid curve) and for observation of autoionization of $2\ ^3\text{S} + 2\ ^3\text{S}$ molecules formed by stimulated two-photon transitions (K_{AI} , dotted curve). (a) Two-laser lineshapes with $I_1 = 100I_{\text{sat}}$, $I_2 = 400I_{\text{sat}}$, and $\Delta_2 = 8$ MHz. (b) Frustrated PA with $I_1 = I_2 = 100I_{\text{sat}}$. Here, Δ_2 is scanned while $\Delta_1 \approx 0$ (corresponding to the peak of the single-laser line, whose height is indicated by the dashed horizontal line). The temperature is $25\ \mu\text{K}$ for all plots.

Autler-Townes doublet, causing a reduction of PA signal. This “frustrated PA” scheme may be convenient for an initial search, as the decrease in PA signal can be made 100%.

At this point, the connection with the experiment described in references [14,15] demands some attention. In this experiment, the PA spectra were obtained in a magnetic trap using a novel calorimetric detection scheme, which is briefly outlined below. Spontaneous decay of the excited state will produce fast atom pairs with energies up to ~ 30 mK, with some of the pairs being in trapped magnetic substates. If the temperature of such atom pairs is below the 10 mK trap depth, their kinetic energy will be deposited in the trapped cloud by rethermalizing collisions. For a sufficiently cold cloud, this leads to substantial heating due to resonant PA, while the decrease in atom number due to the escaping atom pairs may also be detected. Since the heating is related to spontaneous decay of the excited state, the spectra plotted in Figures 3 may also resemble those measured using the calorimetric method. However, although it can be estimated that the above mechanism nearly explains all the heating in the one-laser PA experiments [13,24], other mechanisms

should be considered too. Spontaneous decay of the excited state may also result in a bound $^5\Sigma_g^+$ state, which will eventually decay by autoionization. Due to its small binding energy, the radial wavefunction of the $v = 14$ vibrational state extends far enough to have reasonable FC overlap with the purely long range vibrational states in 0_u^+ , which have classical inner turning points near $150\ a_0$. By contrast, the outer turning points of the vibrational states in $^5\Sigma_g^+$ with $v \leq 13$ lie at internuclear distances smaller than $30\ a_0$ [16]. Therefore, the $v = 14$ state is most likely to be populated via spontaneous decay. Combining a semi-classical estimate of the $v = 14$ vibration frequency with the Penning ionization suppression factor given in reference [25], one arrives at an approximate value for the inverse autoionization-limited lifetime $\Gamma_g = (5\ \mu\text{s})^{-1}$. The autoionization will produce fast He^+ or He_2^+ ions, which may cause heating via collisions with trapped He^* atoms similar to the heating observed in a He^* BEC [5]. This process may become important in the case of stimulated production of $^5\Sigma_g^+$ molecules. To illustrate this, Figures 4 display the rate coefficients K_{AI} for decay by autoionization. Heating due to K_{AI} should be accounted for by multiplying K_{AI} with a certain constant and adding it to K_f to simulate the calorimetric spectrum. Likewise, for the frustrated PA spectrum depicted in Figure 4b, the heating due to $^5\Sigma_g^+$ bound state formation will shallow the dip near $\Delta_2 = 0$. However, as K_{AI} for this case is more than two orders of magnitude smaller than K_f , this effect might be relatively small. The lineshapes for K_{AI} in Figures 4 also suggest the interesting option of ion detection for observing the two-laser transition. Finally, heating due to off-resonant atomic scattering should be taken into account. For intensities of a few hundred I_{sat} , the off-resonant atomic scattering rate can be calculated to be of the same order of magnitude as the PA rate for a cloud at $10^{13}\ \text{cm}^{-3}$ density. Although the photon recoil associated with each atomic scattering event contributes to the heating by about twice the recoil energy (which is small compared to the heating per molecular decay event), the scattering may leave the atom in a different magnetic substate for which Penning ionization is not suppressed. A subsequent Penning ionizing collision may cause significant heating of the cloud. On the other hand, heating due to off-resonant scattering varies slowly with detuning compared to heating due to PA. In a PA experiment, I_1 may be chosen so as to obtain a sufficiently large rate coefficient K_f with a minimum of background signal, thus leading to optimum S/N ratio.

Apparently, the PA signal obtained from heating or loss is related to the strength of the PA process only in an indirect way. This makes the calorimetric detection method less suitable for observing FC oscillations than in reference [11].

The model used here to simulate two-laser PA spectra may also be employed for fitting experimental data. With the temperature known from experiment, the intensity of laser 2 and the binding energy of the $^5\Sigma_g^+$, $v = 14$ level may be used as fit parameters. Moreover, the $\text{He}^* 2\ ^3\text{S} + 2\ ^3\text{P}$ system has good theoretical access: radiative

coupling can be computed using accurate theoretical data, and hyperfine interaction and higher-order partial wave contributions are absent. The two-laser PA spectroscopy proposed in this work may thus serve as an absolute test case for existing theoretical models.

3.2 Optical Feshbach resonance

An OFR requires relatively intense laser fields, which may cause heating or loss of atoms due to off-resonant atomic scattering. Fedichev et al. pointed out that choosing a vibrational level with large binding energy reduces the losses due to atomic scattering, despite the fact that higher intensities will be needed to achieve the same modification of a [17]. The purely long range states below D_0 discussed above have comparatively small binding energies with respect to the D_0 asymptote, and the laser intensity required for an OFR can be estimated to cause strong off-resonant atomic scattering. The subsequent heating and losses would severely limit the lifetime of a cold cloud of atoms, and preclude the use of the purely long range states for an OFR.

As an alternative, the present calculation assumes the existence of a vibrational level with a binding energy of -250 GHz, located in a $(2\ ^3S + 2\ ^3P)\ ^5\Sigma_u^+$ potential below D_2 . The $^5\Sigma_u^+$ potential couples at long-range to the Hund's case (c) states 1_u and 2_u , for which the interaction is well-known [15,26]. The short-range part of this potential has never been considered by experiment or theory. Nevertheless, it is expected that autoionization of this state is strongly suppressed, similar to the suppression of Penning ionization during collisions between spin-polarized He* atoms [12]. The long-range part of the vibrational wavefunction is obtained by inward numerical integration of the radial Schrödinger equation, assuming a binding energy of -250 GHz and taking only the long-range part of the interaction into account. For simplicity, the long-range part is represented by a $-C_3/R^3 - C_6/R^6$ potential (with the dispersion coefficients from Ref. [26]), which has a negligible effect on the wavefunction of the state bound by -250 GHz. The inner part of the excited-state wavefunction thus remains unknown. However, this part of the wavefunction oscillates rapidly with R , and it can be estimated to contribute only marginally to the FC overlap integral involved in the matrix element in equation (2). Now, the effect of PA light (nearly resonant with the vibrational level) on the scattering length and the inelastic loss rate coefficient can be studied using equations (7), (8), and (9). Figure 5 shows the familiar dispersive behaviour of $A = \text{Re } a$ versus detuning (A may even become negative), and the resonant character of K_{inel} . Inelastic losses stem from decay of the excited vibrational level by spontaneous emission, which may result either in fast and/or untrapped atoms or in autoionizing $2\ ^3S + 2\ ^3S$ molecules, or from autoionization of the excited state at short internuclear range.

A more convenient graphical representation of the relation between A and K_{inel} is shown in Figure 6. Here, A and

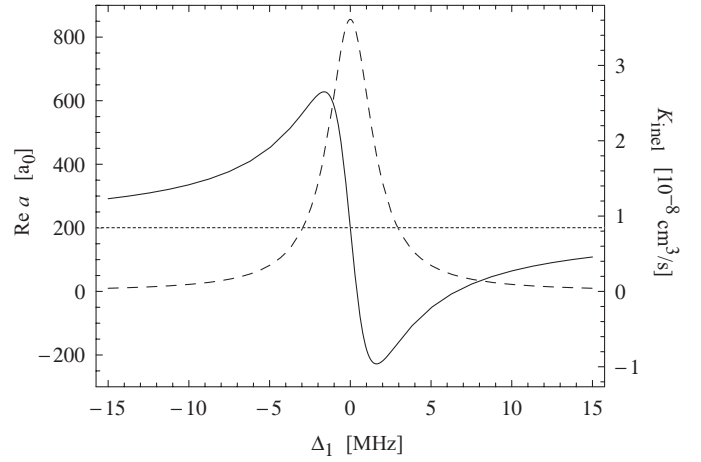


Fig. 5. Optical Feshbach resonance using a PA intensity of 5×10^5 W/m². Solid curve: real part A of the scattering length as a function of detuning away from a vibrational resonance with binding energy -250 GHz. The natural value of the scattering length, a_{nat} , is indicated by the dotted horizontal line and is assumed to be $200 a_0$. Dashed curve: rate coefficient for loss of atoms due to spontaneous decay of the excited state.

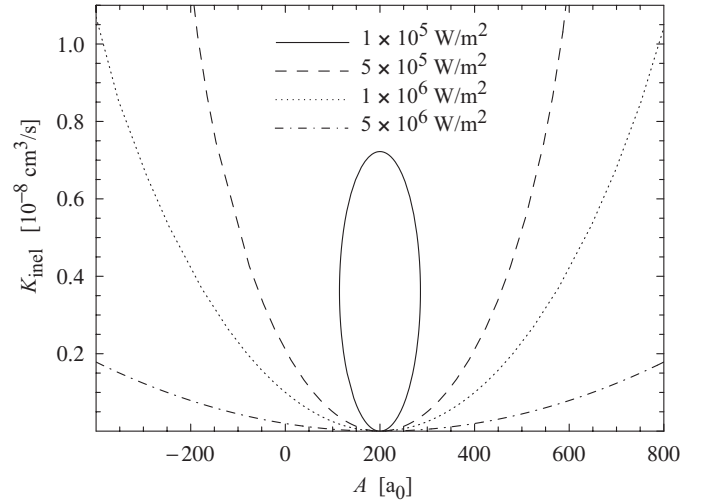


Fig. 6. Parametric plot of K_{inel} versus A , for several PA laser intensities and with Δ_1 being varied as a parameter. Here, a_{nat} is assumed to be $200 a_0$.

K_{inel} are plotted for various PA intensities, with the detuning being varied as a parameter. It is clear that a larger intensity allows for a larger modification of the scattering length at the same level of losses. For the particular case in which A is made to vanish, the losses are seen to *decrease* with increasing PA intensity (here it should be mentioned that for increasing PA intensity, A becomes zero for increasing values of Δ_1). Another crucial role is played by the natural value of the scattering length, a_{nat} . This is illustrated in Figure 7a, where the maximum achievable value for A is plotted as function of PA intensity for several values of a_{nat} lying within the uncertainty of the theoretical prediction [27]. It follows that for a larger value of a_{nat} the modification will be larger too. Similarly, the parameters determining a vanishing value for A depend strongly on a_{nat} as well. As a consequence, the inelastic

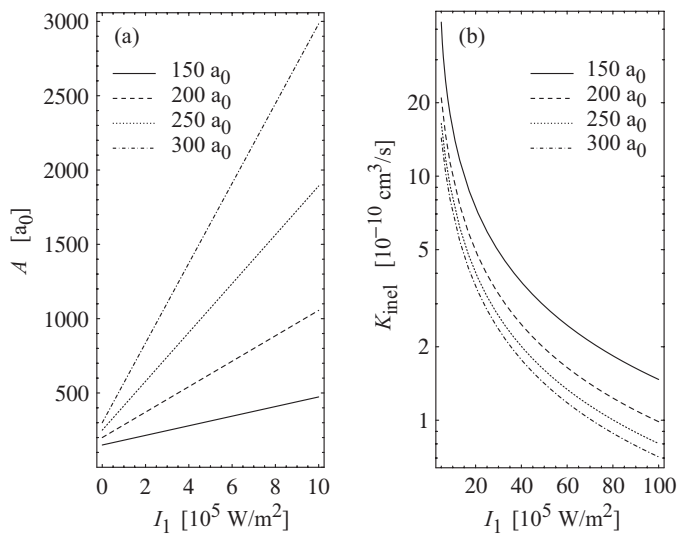


Fig. 7. (a) Maximum achievable value for A versus PA intensity I_1 . The various curves correspond to different values for a_{nat} . (b) Inelastic loss rate coefficient for the case of vanishing A versus PA intensity, for several values of a_{nat} .

loss rate coefficient for the case $A = 0$ decreases with increasing values of a_{nat} , as can be seen in Figure 7b. This strong dependence on a_{nat} emphasizes the importance of an accurate (spectroscopic) determination of the scattering length.

For any of the cases discussed above, the timescale on which the temperature and number of atoms in the cold cloud will be seriously affected is small. For a cloud of He^* atoms at a density of 10^{13} cm^{-3} , PA losses set a timescale of 10^{-5} to 10^{-3} s, whereas off-resonant atomic scattering typically limits the lifetime to several milliseconds or longer. These figures confirm the results of an earlier study of prospects for optical Feshbach resonances in He^* [28]. In fact, the elastic rate never exceeds the inelastic rate by far, and it even is smaller in most of the cases discussed above. This means that the present scheme for optical control of the scattering length can be used only for applications in which short, impulse-like changes of the scattering length are required. For studies of a He^* BEC in an optical lattice, which offers the unique feature of detection of ions produced in Penning collisions, tunability of the scattering length may be interesting [29]. For instance, for the case of two He^* atoms occupying the same lattice site, the PA rate (and thus the modification of a) may be enhanced [30]. This would reduce the losses associated with the conditions which set a to a particular value. Another point of further study may be the behaviour of the Penning collision rate as a function of a .

When designing an experiment to optically control the scattering length, the binding energy of a suitable vibrational level in the excited-state potential should be known. In the case of alkali elements, the location of suitable bound states can often be obtained from existing spectroscopic data on the excited-state potential. In contrast to the case of alkali atoms, helium dimers do not naturally exist, which explains the poor amount of spectro-

scopic data on the $2^3\text{S} + 2^3\text{P}$ states. Theoretical data are available only for the $(2^3\text{S} + 2^3\text{P})^3\Sigma_g^+$ state; data of singlet and quintet molecular potential energy curves have hitherto not been published. To avoid an extensive spectroscopic search for lines near the desired binding energy, the accumulated-phase method might be employed to assist in predicting their locations [12,31]. For an accurate prediction of vibrational level positions, however, the availability of ab initio data is probably crucial.

When deciding on a suitable vibrational level to use for an optical Feshbach resonance, a point of concern is whether nearby molecular vibrational resonances in singlet or triplet potentials can be excited by the PA light. Such resonances, which will be broadened to almost the vibrational level spacing because of the large (near unity) probability of autoionization at short range [32], introduce additional losses. However, for the Condon radius corresponding to excitation at -250 GHz, all nearby molecular potentials are nearly pure Hund's case (a) states, as the relativistic atomic interactions that mix them at long range are small compared to the resonant dipole-dipole interaction. Starting from a sample of spin-polarized He^* atoms, this means that only quintet *ungerade* states can be accessed, and no PA to molecular states coupling to strongly autoionizing singlet and triplet configurations is possible.

4 Conclusion

Two-laser PA spectroscopy of ultracold spin-polarized He^* atoms, aiming at the detection of the least-bound vibrational level in the $^5\Sigma_g^+$ scattering potential, has been investigated numerically. The binding energy of this state may be used to infer an accurate value for the He^* s -wave scattering length. The scheme, which assumes the purely long range $v = 0$ vibrational level in the 0_u^+ potential well below D_0 as the intermediate level, may result in a detectable two-photon stimulated Raman transition for feasible experimental parameters. Different approaches to observe the two-laser transition are discussed within the context of a calorimetric detection method [14,15].

In addition, optical control of the He^* scattering length using optical Feshbach resonances has been explored numerically. Modification of the scattering length to very large ($>10^3 a_0$) values or to vanishing or even negative values is anticipated for experimentally realizable conditions, although the magnitude of the optical Feshbach resonance depends strongly on the natural value of the scattering length. Also, this method to control the scattering length may be applied only for a very short (10^{-5} to 10^{-3} s) duration, to avoid substantial loss and/or heating of trapped atoms. This will undoubtedly complicate a possible experimental implementation of an OFR. Notwithstanding all the experimental disadvantages as compared to magnetic Feshbach resonances, optical Feshbach resonances are presumably the only handle one has to modify the value of the He^* scattering length. Finally, several experimental issues concerning the search for and choice of a suitable excited-state vibrational level have been discussed.

Allard Mosk is gratefully acknowledged for useful comments on the manuscript and fruitful discussions. The authors further wish to thank the members of the ultracold metastable helium team at École Normale Supérieure (ENS), Jérémie Léonard, Olivier Dulieu, and Servaas Kokkelmans for stimulating conversations. The stay of J.K. at ENS was financially supported by means of a Marie Curie European fellowship.

Appendix: Matrix elements of the radiative coupling

The matrix element in equation (2) involves the energy-normalized state $|f_E\rangle$ (the label l is dropped since only the $l = 0$ contribution is taken into account), which can be written as the product of a radial wavefunction, a rotationless angular part, and the rotational part of the molecular state:

$$|f_E\rangle = \frac{u_{f,E}(R)}{R} |^5\Sigma_g^+\rangle |J\Omega M\rangle. \quad (10)$$

Here, Ω is the projection of J on the internuclear axis, whereas M is the projection of J on the lab-fixed z -axis, defined by the field of the magnetic trap. For spin-polarized He* atoms, $M = 2$; hence $J = 2$ (for $l = 0$). Ω depends on the alignment of the internuclear axis with respect to the z -axis. The energy-normalized radial wavefunction, $u_{f,E}(R)$, is obtained by solving the Schrödinger equation for two free atoms in the scattering potential with an asymptotic energy E , with the long-range boundary condition [19]

$$u_{f,E}(R) \sim \sqrt{\frac{2\mu}{\pi\hbar^2k}} \sin[kR + \eta(k)], \quad R \rightarrow \infty. \quad (11)$$

Here k is the initial wave number, and $\eta(k)$ denotes an energy-dependent phase shift. The left-hand side of equation (11) corresponds to an energy-normalized, free-particle state. The excited bound state can be written as

$$\begin{aligned} |e\rangle &= \frac{u_{v=0}(R)}{R} |0_u^+\rangle |J'\Omega'M'\rangle \\ &= \frac{u_{v=0}(R)}{R} \left\{ c_1(R) |^5\Sigma_u^+\rangle + c_2(R) |^5\Pi_u\rangle \right. \\ &\quad \left. + |\text{n.c.}\rangle \right\} |J'\Omega'M'\rangle, \end{aligned} \quad (12)$$

where $c_i(R)$ are the expansion coefficients of $|0_u^+\rangle$ expressed in *ungerade* Hund's case (a) states. |n.c.) is the sum of all singlet and triplet states in the expansion $|0_u^+\rangle$, which are not coupled to the $^5\Sigma_g^+$ lower state by a dipole transition. Therefore, these states may be omitted in the evaluation of the matrix element of V_{rad} . Bose statistics furthermore require that $J' = 1$. Consequently, because of dipole selection rules, only the $M' = 1$ state can be excited starting from the $M = 2$ lower state, which implies σ^- transitions induced by laser 1.

The matrix element involves a spatial integration, which can be split up in an angular part and a radial part

(the so-called *Franck-Condon integral*). It should be noted that the Franck-Condon *principle* (i.e. approximating the integral by replacing it with the integrand evaluated at the Condon radius) does not apply to the transition to the $v = 0$ excited state in 0_u^+ . This is due to the fact that the $v = 0$ radial wavefunction, unlike more highly excited vibrational wavefunctions, has a broad amplitude maximum which spans the entire classically allowed region. Also, a common approximation in which only the radial wavefunctions $u(R)$ in the FC integral are included is inadequate, since the angular part of the matrix element also depends on R via the expansion coefficients $c_i(R)$ in equation (12). The FC integral is therefore evaluated over the full internuclear range of overlap, including the radial wavefunctions and expansion coefficients $c_i(R)$, with each coefficient weighted by the value of the corresponding angular part of the matrix element. The latter is evaluated using the direction cosine matrix [33,34]. It should also be noted that the atomic dipole moment in equation (3) is modified so as to take the presence of the magnetic field (which lifts the degeneracy of the lower state) into account.

For the matrix element describing the radiative coupling in the OFR, the radial integration is limited to the internuclear range for which the excited-state wavefunction is known (Sect. 3.2), thereby neglecting the short-range contribution. Since in this case the excited state is virtually a pure Hund's case (a) state, the radial integral only contains the radial wavefunctions of the lower and excited states.

The bound-bound matrix element in equation (4) is obtained along the same lines as given above, but now involving an $M' = 1 \rightarrow M = 2$ transition. It is furthermore assumed that the magnetic moment of the $v = 14$ bound state in the $^5\Sigma_g^+$ potential is identical to that of the initial free-atom pair, such that all Zeeman shifts due to the field of the magnetic trap cancel out.

References

1. A. Robert, O. Sirjean, A. Browaeys, J. Poupard, S. Nowak, D. Boiron, C.I. Westbrook, A. Aspect, *Science* **292**, 461 (2001)
2. O. Sirjean, S. Seidelin, J.V. Gomes, D. Boiron, C.I. Westbrook, A. Aspect, G.V. Shlyapnikov, *Phys. Rev. Lett.* **89**, 220406 (2002)
3. S. Seidelin, O. Sirjean, J.V. Gomes, D. Boiron, C.I. Westbrook, A. Aspect, *J. Opt. B: Quant. Semiclass. Opt.* **5**, S112 (2003)
4. F.X. Gadea, T. Leininger, A.S. Dickinson, *J. Chem. Phys.* **117**, 7122 (2002)
5. F. Pereira Dos Santos, J. Léonard, Junmin Wang, C.J. Barrelet, F. Perales, E. Rasel, C.S. Unnikrishnan, M. Leduc, C. Cohen-Tannoudji, *Phys. Rev. Lett.* **86**, 3459 (2001)
6. M. Leduc, J. Léonard, F. Pereira dos Santos, E. Jahier, S. Schwartz, C. Cohen-Tannoudji, *Act. Phys. Pol. B* **33**, 2213 (2002)
7. S. Seidelin, J. Viana Gomes, R. Hoppeler, O. Sirjean, D. Boiron, A. Aspect, C.I. Westbrook, *Phys. Rev. Lett.* **93**, 090409 (2004)

8. P.J.J. Tol, W. Hogervorst, W. Vassen, Phys. Rev. A **70**, 013404 (2004)
9. E.R.I. Abraham, W.I. McAlexander, C.A. Sackett, R.G. Hulet, Phys. Rev. Lett. **74**, 1315 (1995)
10. H. Wang et al., Phys. Rev. A **62**, 052704 (2000)
11. J.R. Gardner, R.A. Cline, J.D. Miller, D.J. Heinzen, H.M.J.M. Boesten, B.J. Verhaar, Phys. Rev. Lett. **74**, 3764 (1995)
12. J. Léonard, P. van der Straten, A.P. Mosk, M. van Rijnbach, M. Walhout, D. Nehari, M. Leduc, Phys. Rev. A (in preparation)
13. J. Kim, U.D. Rapol, S. Moal, J. Léonard, M. Walhout, M. Leduc, Eur. Phys. J. D **31**, 227 (2004)
14. J. Léonard, M. Walhout, A.P. Mosk, T. Müller, M. Leduc, C. Cohen-Tannoudji, Phys. Rev. Lett. **91**, 073203 (2003)
15. J. Léonard, A.P. Mosk, M. Walhout, P. van der Straten, M. Leduc, C. Cohen-Tannoudji, Phys. Rev. A **69**, 032702 (2004)
16. J. Stärck, W. Meyer, Chem. Phys. Lett. **225**, 229 (1994)
17. P.O. Fedichev, Yu. Kagan, G.V. Shlyapnikov, J.T.M. Walraven, Phys. Rev. Lett. **77**, 2913 (1996)
18. M. Theis, G. Thalhammer, K. Winkler, M. Hellwig, G. Ruff, R. Grimm, J. Hecker Denschlag, preprint [arXiv:cond-mat/0404514](https://arxiv.org/abs/cond-mat/0404514) (2004)
19. J.L. Bohn, P.S. Julienne, Phys. Rev. A **60**, 414 (1999)
20. R. Napolitano, J. Weiner, C.J. Williams, P.S. Julienne, Phys. Rev. Lett. **73**, 1352 (1994)
21. J.L. Bohn, P.S. Julienne, Phys. Rev. A **56**, 1486 (1997)
22. R.W. Montalvão, R. Napolitano, Phys. Rev. A **64**, 011403(R) (2001)
23. A. Simoni, P.S. Julienne, E. Tiesinga, C.J. Williams, Phys. Rev. A **66**, 063406 (2002)
24. J. Léonard, thèse de Doctorat, Université Marie Curie — Paris 6 (2003), electronic version on line: <http://tel.ccsd.cnrs.fr/>
25. P.O. Fedichev, M.W. Reynolds, U.M. Rahmanov, G.V. Shlyapnikov, Phys. Rev. A **53**, 1447 (1996)
26. V. Venturi, P.J. Leo, E. Tiesinga, C.J. Williams, I.B. Whittingham, Phys. Rev. A **68**, 022706 (2003)
27. In the calculation, a_{nat} is varied by slight modification of the dispersive long-range part of the $^5\Sigma_g^+$ scattering potential
28. A.P. Mosk, *Photoassociation of magnetically trapped metastable He*, internal report, École Normale Supérieure, Paris (2002)
29. P.O. Fedichev, M.J. Bijlsma, P. Zoller, Phys. Rev. Lett. **92**, 080401 (2004)
30. D. Jaksch, V. Venturi, J.I. Cirac, C.J. Williams, P. Zoller, Phys. Rev. Lett. **89**, 040402 (2002)
31. A.J. Moerdijk, W.C. Stwalley, R.G. Hulet, B.J. Verhaar, Phys. Rev. Lett. **72**, 40 (1994)
32. M.W. Müller, A. Merz, M.W. Ruf, H. Hotop, W. Meyer, M. Movre, Z. Phys. D **21**, 89 (1991)
33. J.T. Hougen, *The calculation of rotational energy levels and rotational line intensities in diatomic molecules*, Natl. Bur. Stand. monograph 115 (U.S. GPO, Washington, D.C. 1970), <http://physics.nist.gov/Pubs/Mono115>
34. H. Lefebvre-Brion, R.W. Field, *Perturbations in the spectra of diatomic molecules* (Academic Press, London, 1986)